PHYSICAL REVIEW B VOLUME 59, NUMBER 16 15 APRIL 1999-II

Density matrix of inelastically scattered fast electrons

P. Schattschneider
Institut für Angewandte und Technische Physik, University of Technology Wien, A-1040 Vienna, Austria

M. Nelhiebel and B. Jouffrey
LMSSMat, CNRS-URA 850, École Centrale Paris, F-92295 Châtenay-Malabry, France

(Received 15 May 1998)

The kinetic equation for the evolution of a fast electron's density matrix ρ after single inelastic scattering is solved in the one-beam approximation. The solution holds for any type of inelastic interaction and for any scatterer. It relates ρ directly to the mixed dynamic form factor (MDFF) for inelastic scattering, which in turn is the Fourier transform of an energy-loss dependent density correlation function. This approach allows simulations of both energy-filtered diffraction patterns and high-resolution energy spectroscopic imaging (ESI), as well as access to the mutual coherence and the density autocorrelation function of the probe electron, all under the same formalism and the same approximation. A criterion for the maximum attainable resolution in ESI is derived. As an example, we discuss dipole-allowed atomic transitions for the Si-K ionization.
[S0163-1829(99)08615-4]

I. INTRODUCTION

The key quantity for the description of inelastic scattering of fast electrons in crystals is the mixed dynamic form factor (MDFF). It is a generalization of the more familiar dynamic form factor that describes single inelastic scattering of a single incident plane wave. The generalization is stipulated because in crystals, the inelastically scattered wave consists of a number of mutually coherent plane waves, and interference terms should occur. These very terms are described by the MDFF. They are particularly important in core-loss spectrometry.

Although the MDFF has been used for nearly half a century in electron microscopy in different contexts and disguises (see Refs. 1–6), it still seems to be considered merely as a mathematical expression without much relevance to the underlying physics. We grant that for the calculation of inelastic scattering cross sections in crystals it is not necessary to understand what the MDFF represents. However, an understanding of its physical significance sheds light onto what is important in inelastic interactions. Moreover, it describes the formation of both energy filtered images and energy spectroscopic diffraction patterns under the same formalism.[7,8]

The aim of this paper is to provide a physical understanding of the MDFF and its relation to the density matrix, and to demonstrate what can be achieved therefrom. We shall deliberately choose a simple demonstration example.

We begin with a definition of the MDFF, which lends itself to a clear physical interpretation. We shall see that it is closely related to the density matrix[9–12] of the scatterer. Thereafter, we discuss the relation between the MDFF and the densiy matrix of the scattered electron. This has important consequences for the simulation of electron spectroscopic diffraction patterns and high resolution images obtained from inelastically scattered electrons. Finally, we demonstrate the applicability of this concept for inelastic electron scattering by discussion of the electron distribution at the exit plane of the specimen after an ionization of a single atom.

II. THE MIXED DYNAMIC FORM FACTOR

In the first Born approximation, and for an incident plane wave, the double differential scattering cross section is[13]

$$\frac{\partial^2\sigma}{\partial E\,\partial\Omega}=\frac{4\gamma^2}{q^4a_0^2}\frac{k}{k_0}S(\mathbf{q},\mathbf{q},E), \tag{1}$$

where $a_0=4\pi\varepsilon_0\hbar^2/me^2$ is the Bohr radius, and γ is a relativistic factor. $S(\mathbf{q},\mathbf{q}',E)$ is the mixed dynamic form factor. The more often used dynamic form factor—which actually appears in Eq. (1)—is the diagonal element ($\mathbf{q}=\mathbf{q}'$) of the MDFF. For reasons which become clear in the following, we prefer to use here the more general MDFF. The three-dimensional variable $\mathbf{q}$ is a vector in reciprocal space, related to the solid angle Ω appearing on the left hand side by the scattering geometry: ϑ is the angle between the incident electrons' wave vector $\mathbf{k}_0$ and $\mathbf{k}_0+\mathbf{q}$. Energy conservation requires that for a given energy loss E the dynamic form factor $S(\mathbf{q},\mathbf{q},E)$ vanishes except when the wave vector of the scattered electron is $\mathbf{k}=\mathbf{q}+\mathbf{k}_0$. We shall distinguish the quantity $\mathbf{Q}=\mathbf{k}-\mathbf{k}_0$ from an arbitrary vector $\mathbf{q}$ in reciprocal space. Note that $-\hbar\mathbf{Q}$ is the momentum transferred to the scatterer in the inelastic interaction.

For an n-electron system the MDFF reads[7]

$$S(\mathbf{q},\mathbf{q}',E)=\delta(E+E_i-E_f)\sum_i p_i\sum_f(1-p_f)\times\left\langle i\left|\sum_j^n e^{i\mathbf{q}\hat{\mathbf{R}}_j}\right|f\right\rangle\left\langle f\left|\sum_l^n e^{-i\mathbf{q}'\hat{\mathbf{R}}_l}\right|i\right\rangle. \tag{2}$$

Each term in the sum is the product of two transition probability amplitudes of the target, from an initial state $|i\rangle$ to a final state $|f\rangle$ with occupation probabilities p_i, p_f. The transitions are caused by the respective operators $\Sigma_j^n e^{i\mathbf{q}\hat{\mathbf{R}}_j}$, and $\Sigma_l^n e^{i\mathbf{q}'\hat{\mathbf{R}}_l}$. The delta function guarantees that the energy difference between initial and final states be constant, $E_f - E_i = E$. $\hat{\mathbf{R}}_j$ is the space operator of the jth particle.

A. The *r* MDFF for one-electron transitions

In the remaining section, we restrict the discussion to one-electron transitions, in order to facilitate the interpretation. In this case, the sums over space operators reduce to one term,[14] and $|i\rangle, |f\rangle$ are one-electron wave functions.

We shall make use of Fourier transforms in the following. For convenience we use the notation

$$f(\mathbf{r}) = FT_{\mathbf{q}}[f(\mathbf{q})] := \frac{1}{(2\pi)^n}\int d^n q\, f(\mathbf{q}) e^{i\mathbf{q}\mathbf{r}}, \tag{3}$$

where n is 1, 2, 3, depending on the dimension of the vector $\mathbf{q}$. The inverse transform is

$$f(\mathbf{q}) = FT_{\mathbf{r}}[f(\mathbf{r})] = \int d^n r\, f(r) e^{-i\mathbf{q}\mathbf{r}}. \tag{4}$$

Henceforth $\mathbf{r}$, $\mathbf{x}$, and the primed quantities denote vectors in two- or three-dimensional space, and $\mathbf{q}$, $\mathbf{k}$, and the primed quantities are two- or three-dimensional vectors in reciprocal space. The Fourier transform of the MDFF with respect to $\mathbf{q}$, $-\mathbf{q}'$ shall be denoted as *r* MDFF, in order to distinguish it from its usual form in reciprocal space. With

$$FT_{\mathbf{q}}[e^{i\mathbf{q}\hat{\mathbf{R}}}] = \delta^n(r - \hat{\mathbf{R}}) \tag{5}$$

and

$$FT_q[f(q)]^* = FT_{-q}[f^*(q)] \tag{6}$$

the *r* MDFF—the Fourier transform of Eq. (2)—is

$$\begin{aligned} S(\mathbf{r},\mathbf{r}',E) &= FT_{\mathbf{q},-\mathbf{q}'}[S(\mathbf{q},\mathbf{q}',E)] \\ &= \sum_i p_i \sum_f (1-p_f)\langle i|\delta^3(\mathbf{r}-\hat{\mathbf{R}})|f\rangle \\ &\quad \times \langle f|\delta^3(\mathbf{r}'-\hat{\mathbf{R}})|i\rangle \delta(E+E_i-E_f). \end{aligned} \tag{7}$$

Note that we transformed with respect to $-\mathbf{q}'$. This was necessary because the matrix element containing $\mathbf{q}'$ is the complex conjugate of the matrix element containing $\mathbf{q}$. In real-space representation—usually achieved by insertion of $\int d^3R|\mathbf{R}\rangle\langle\mathbf{R}|$—this is

$$\begin{aligned} S(\mathbf{r},\mathbf{r}',E) &= \sum_i p_i \sum_f (1-p_f) \\ &\quad \times \int d^3R\, \phi_i^*(\mathbf{R})\delta^3(\mathbf{r}-\mathbf{R})\phi_f(\mathbf{R}) \\ &\quad \times \int d^3R'\, \phi_i(\mathbf{R}')\delta^3(\mathbf{r}'-\mathbf{R}') \\ &\quad \times \phi_f^*(\mathbf{R}')\delta(E+E_i-E_f) \\ &= \sum_i p_i \phi_i^*(\mathbf{r})\phi_i(\mathbf{r}') \\ &\quad \times \sum_f (1-p_f)\phi_f(\mathbf{r})\phi_f^*(\mathbf{r}')\delta(E+E_i-E_f). \end{aligned} \tag{8}$$

The sum over i collects all occupied states, the sum over f all unoccupied states of the system, with the important constraint of a fixed energy difference E between initial and final states imposed by the delta function. This latter sum then includes exactly the states the scatterer can be in after transitions with fixed energy difference.

We define the energy—dependent density matrix of the target initial state consisting of all originally occupied eigenfunctions as

$$\rho_i(\mathbf{r},\mathbf{r}',E) := \sum_j p_j \phi_j^*(\mathbf{r})\phi_j(\mathbf{r}')\delta(E-E_j), \tag{9}$$

where E_j is the energy level of state ϕ_j. An equivalent expression holds for the final state. When the scatterer is in thermal equilibrium, each term is weighted with the thermodynamic factor[8] $p_j = (1/\mathcal{Z})e^{-E_j/k_BT}$.

Since at room temperature or below the thermal smearing of the Fermi edge is negligible as compared to the energy scale between atomic levels, $p_f \approx \Theta(E_F - E)$, the density matrix of the target final state can be approximated by

$$\rho_f(\mathbf{r},\mathbf{r}',E) \doteq \sum_{E_j>E_F} \phi_j^*(\mathbf{r})\phi_j(\mathbf{r}')\delta(E-E_j). \tag{10}$$

Note that Eq. (9) is also valid for nonequilibrium conditions when the proper occupation numbers are used.[15]

With Eqs. (9) and (10) the *r* MDFF, Eq. (8) can be written as an integral over energy of two matrix elements of density matrices. As the zero level, we choose the Fermi energy. Collecting terms in Eq. (8),

$$S(\mathbf{r},\mathbf{r}',E) = \int_{-E}^{0} \rho_i(\mathbf{r},\mathbf{r}',\varepsilon)\rho_f(\mathbf{r}',\mathbf{r},\varepsilon+E)\,d\varepsilon. \tag{11}$$

The *r* MDFF is the energy correlation function between the denstity matrices of occupied (initial) states and unoccupied (final) states, with energy difference E between these states. E equals the energy loss of the probe electron. This is the physical meaning of the *r* MDFF.

This is an important result because it relates the rather abstract quantity of the MDFF to electron densities of the scatterer. It is the overlap of initial and final electron densities and correlations that governs the outcome of inelastic scattering experiments. Given that the initial-state wave functions are known, Eq. (11) can be used to extract information on final-state wave functions from scattering experiments.

B. The MDFF in a crystal

Equation (11) is most easily applied to single atoms where the wave functions can be calculated without too much difficulty. The MDFF of an ensemble of noninteracting atoms can as well be calculated from Eq. (11). Since the initial wave functions of adjacent atoms don't show phase relations (they dont see each other) the r MDFF of such an ensemble is simply the sum over atomic r MDFF's:

$$S(\mathbf{r},\mathbf{r}',E)_{cluster}=\sum_{i}^{N} S_i(\mathbf{r}-\mathbf{r}_i,\mathbf{r}'-\mathbf{r}_i,E). \tag{12}$$

Invoking the shift theorem for Fourier transforms, we transform Eq. (12) to

$$S(\mathbf{q},\mathbf{q}',E)_{cluster}=\sum_{i}^{N} e^{i(\mathbf{q}-\mathbf{q}')\mathbf{r}_i}S_i(\mathbf{q},\mathbf{q}',E). \tag{13}$$

In a crystal, the final states are no longer atomic wave functions, but include the full electronic band structure derived from the periodic potential; the initial states can be considered to remain unchanged. We can then still add r MDFF's as in Eq. (12) where the S_i has to be replaced by the MDFF of the motif in a single elementary cell:

$$S_{motif}(\mathbf{q},\mathbf{q}',E)=\sum_{\mathbf{u}} e^{i(\mathbf{q}-\mathbf{q}')\mathbf{u}}S_{\mathbf{u}}(\mathbf{q},\mathbf{q}',E), \tag{14}$$

where $S_{\mathbf{u}}$ is the MDFF of the uth atom in the elementary cell, calculated with the full electronic band structure. Letting $N \to\infty$ in Eq. (13), the sum becomes a Dirac comb in reciprocal space:

$$S(\mathbf{q},\mathbf{q}',E)_{crystal}=S_{motif}(\mathbf{q},\mathbf{q}',E)\sum_{j} \delta^3(\mathbf{q}-\mathbf{q}'-\mathbf{g}_j). \tag{15}$$

In other words, the MDFF of such a crystal vanishes except when $\mathbf{q}-\mathbf{q}'$ equals a vector $\mathbf{g}_j$ of the reciprocal lattice.[7] For $\mathbf{q}=\mathbf{q}'$, Eq. (15) reduces to $S_{crystal}=S_{motif}$. The diagonal element of the MDFF in a crystal (or, the direct term, as we call it) equals that of the elementary motif. Contrary to the elastic case, the lattice periodicity is directly visible only in the skew diagonal elements, i.e., it changes only the mutual coherence of the outgoing electron by the delta function in Eq. (15). Its angular distribution is the same as that obtained after scattering on the elementary motif.

III. THE DENSITY MATRIX OF THE INCIDENT ELECTRON

The double differential scattering cross section as given by Eq. (1) measures the momentum probability distribution after inelastic scattering of a fast electron that can be described by an incident plane wave. It relates to the diagonal element of the MDFF. Thus from scattering experiments we get important information on the scatterer, namely on the diagonal elements of its energy dependent density matrices.

But we can also put it the other way around: the dynamic structure factor of the scatterer determines the momentum distribution of the probe electron. The general question is then: given the MDFF, what information on the energy dependent density matrix *of the probe electron* can be extracted? And can we tell whether the probe electron after inelastic scattering is in a pure or in a mixed state? In elastic scattering, the first problem is equivalent to the problem of how to simulate diffraction patterns or high-resolution (HR) images from a model potential of the scatterer, related to the static form (or structure) factor $F(\mathbf{q})$. Knowledge of the complex quantity F allows calculation of the scattering profile via $|F(\mathbf{q})|^2$ as well as of HR images via $|\tilde{F}(\mathbf{r})|^2$ where F and $\tilde{F}$ are related by a Fourier transform.

Here, we encounter the phase problem: in order to obtain information on the spatial charge distribution, we need the phase of F [or, differently posed, the matrix $F(\mathbf{q})\cdot F^*(\mathbf{q}')$]. The second problem is immediately solved for elastic scattering: Since $F(\mathbf{q})\cdot F^*(\mathbf{q}')$ factorizes into q- and q'-dependent functions, the same is true for the density matrix of the scattered electron, so the electron is in a pure state. The difference to inelastic scattering is that $S(\mathbf{q},\mathbf{q}',E)$ does not, in general, decompose into two factors each of which depends on a single momentum variable only, and the electron might be in a mixed state.

A. The single-scattering one-beam case

We shall now derive a relation between the MDFF of the scatterer and the density matrix of the probe electron, under particular conditions that allow a simple interpretation of the MDFF, namely the single inelastic scattering, one-beam case (i.e., we assume that the incident electron is a monochromatic plane wave, and that the specimen is so thin that only one inelastic scattering process takes place, and there is no elastic scattering, neither before nor after the inelastic interaction). This is fulfilled when the specimen thickness is much smaller than the extinction distance for the excited Bragg beams. Although our primary aim is to provide physical insight into the concept of the MDFF, and thus the approximations are chosen mainly for didactic reasons, our above assumptions are more realistic than one would believe at first glance. Quantification routines, e.g., are based on exactly the single-scattering one-beam case. Furthermore, a generalization to the case of Bragg scattering is straightforward, but would hide the physical significance of our results.

We start from the kinetic equation given by Dudarev, Peng, and Whelan.[8] It describes the propagation of the density matrix of an incident wave in a crystal, including inelastic scattering, under fairly general conditions. Here we simplify by assuming a thin crystal of only a few atomic layers, and fast incident electrons of 100 keV or more. In this regime, the single-scattering approximation is valid (mean free paths for inelastic scattering are of the order of >50 nm.) It is further assumed that the incident electrons are monochromatic, and we look at one fixed energy loss $E>0$. Then, the kinetic equation for the energy dependent density matrix of the inelastically scattered electron after energy loss E,

$$\rho_E(\mathbf{r},\mathbf{r}'):=\rho(\mathbf{r},\mathbf{r}',E_0-E), \tag{16}$$

is

$$\rho_E(\mathbf{r},\mathbf{r}') = \int d^3x d^3x' G_k(\mathbf{r},\mathbf{x}) G_k^*(\mathbf{r}',\mathbf{x}') K(\mathbf{x},\mathbf{x}',E) \rho_0(\mathbf{x},\mathbf{x}'). \tag{17}$$

The inelastic scattering is described by the function

$$K(\mathbf{x},\mathbf{x}',E) = \frac{e^4}{\varepsilon_0^2} FT_{\mathbf{q},-\mathbf{q}'}\left[\frac{S(\mathbf{q},\mathbf{q}',E)}{q^2 q'^2}\right] \tag{18}$$

with the elementary charge e and the vacuum permittivity ε_0. (In cgs units, $\varepsilon_0 = 1/4\pi$.) The incident wave is given by its density matrix $\rho_0(\mathbf{x},\mathbf{x}')$ which for a single incident plane wave of wave vector $\mathbf{k_0}$ is

$$\rho_0(\mathbf{x},\mathbf{x}') = e^{i\mathbf{k_0}\mathbf{x}} e^{-i\mathbf{k_0}\mathbf{x}'}. \tag{19}$$

The function K accounts for inelastic scattering at positions $\mathbf{x},\mathbf{x}'$, and the two Green functions propagate the scattered state from positions $\mathbf{x},\mathbf{x}'$ to positions $\mathbf{r},\mathbf{r}'$. We calculate now the density matrix of the probe electron in reciprocal space, after inelastic scattering:

$$\rho_E(\mathbf{q},\mathbf{q}') = FT_{\mathbf{r},-\mathbf{r}'}[\rho_E(\mathbf{r},\mathbf{r}')] \tag{20}$$

by Fourier transforming the kinetic Eq. (17).

The density matrix $\overline{\rho_E}(\mathbf{q}_x,\mathbf{q}_x')$ of the probe electron in the diffraction plane with two-dimensional coordinates $\mathbf{q}_x$ is then [see Appendix A, Eq. (A8)]

$$\overline{\rho_E}(\mathbf{q}_x,\mathbf{q}_x') = \left(\frac{2\pi m e^2}{\varepsilon_0 \hbar^2 k}\right)^2 \frac{S(\mathbf{Q},\mathbf{Q}',E)}{Q^2 Q'^2} \tag{21}$$

with

$$\mathbf{Q} = \begin{pmatrix} \mathbf{q}_x \\ q_E \end{pmatrix} \tag{22}$$

and equivalently for the primed variable. $q_E = k - k_0$ is the negative difference of radii of the Ewald spheres before and after inelastic scattering. For small energy losses $E \ll E_0$ we have approximately $q_E \approx -k_0 E/2E_0$.

This is our basic result. It relates the density and the mutual coherence of the inelastically scattered electron to the MDFF of the scatterer, in a simple and clear manner. It allows calculation of both the density and the coherence of the probe electron when the MDFF is known, and vice versa.

B. The differential scattering cross section

The scattering cross section is the differential current of scattered particles divided by the incident-particle current density

$$j_0 = \int \rho_0(\mathbf{q}_x,\mathbf{q}_x) d^2 q_x. \tag{23}$$

According to the normalization of the incident wave, Eq. (19),

$$j_0 = (2\pi)^4 a k_0, \tag{24}$$

where a is a proportionality constant. The differential current of scattered particles is similarly

$$\frac{\partial^2 J}{\partial E \partial^2 q_x} = a k \rho_E(\mathbf{q}_x,\mathbf{q}_x). \tag{25}$$

We obtain for the cross section

$$\frac{\partial^2 \sigma}{\partial E \partial \Omega} = \frac{a k \rho_E(\mathbf{q}_x,\mathbf{q}_x)}{j_0} \frac{d^2 q_x}{d\Omega} = \frac{k}{k_0}\left(\frac{2 m e^2}{4\pi\varepsilon_0 \hbar^2}\right)^2 \frac{S(\mathbf{Q},\mathbf{Q},E)}{Q^4}.$$

With the definition of the Bohr radius this is again Eq. (1).

Eq. (21) relates the density matrix after single inelastic scattering to the MDFF. This allows calculation of high-resolution images obtained from inelastically scattered electrons. In practice, the one-beam approximation will not hold, and a more realistic Green function for wave propagation in a periodic potential must be used.[8,16] Still, the one-beam single-scattering approximation for atomic transitions might be useful for very thin specimens where dynamical scattering is unimportant. Preliminary estimates set the limit to a crystal thickness of about 30% of the extinction distance.

Eqs. (8) and (21) allow in principle to calculate the density matrix of the probe electron from knowledge of the wave functions of the scatterer. The diagonal elements describe the momentum distribution of the inelastically scattered electron. But there is much more information contained. We also have the mutual coherence in the angular intensity distribution after scattering. So to speak, knowledge of the density matrix solves the phase problem for inelastic electron scattering. The density matrix shows immediately the angular difference over which two beams leaving the specimen are mutually coherent. Moreover, as we shall see, a double Fourier transform delivers the density matrix in r space, i.e., both the charge density distribution at the exit plane of the specimen, as well as the mutual coherence between two positions.

C. The density matrix in real space

We return now to the density matrix in real space. The density matrix of the scattered electron in r space, immediately after the exit plane of the specimen, is Eq. (17) for $z = 0$, $z' = 0$. Equivalently, we can calculate the two-dimensional Fourier transform of Eq. (21):

$$\overline{\rho_E}(\mathbf{x},\mathbf{x}') = FT_{\mathbf{q}_x,-\mathbf{q}_x'}[\overline{\rho_E}(\mathbf{q}_x,\mathbf{q}_x')]. \tag{26}$$

This corresponds to the transform from the diffraction plane to the image plane in the electron microscope, provided we have a perfect lens.

With the convolution theorem, Eq. (21) reads

$$\overline{\rho_E}(\mathbf{x},\mathbf{x}') = \left(\frac{2\pi m e^2}{\varepsilon_0 \hbar^2 k}\right)^2 FT_{\mathbf{q}_x}[Q^{-2}] FT_{-\mathbf{q}_x'}[Q'^{-2}] * \times FT_{\mathbf{q}_x,-\mathbf{q}_x'}[S(\mathbf{Q},\mathbf{Q}',E)]. \tag{27}$$

The asterisk denotes convolution. The Fourier transform of the prefactor is easily found to be the modified Bessel function K_0 (see Appendix B):

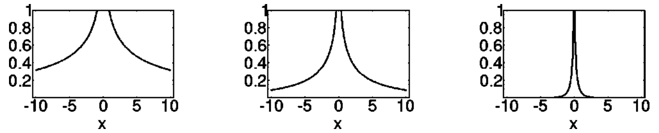

FIG. 1. Contrast of an object with pointlike *r* MDFF and perfect imaging system, for an energy loss of (a) 17 eV; (b) 100 eV; and (c) 1850 eV. Abscissa in atomic units.

$$FT_{\mathbf{q}_x}[Q^{-2}]=K_0(xq_E). \tag{28}$$

Noting that

$$FT_z[f(\mathbf{r})]=FT_{\mathbf{q}_x}[\tilde{f}(\mathbf{q})] \tag{29}$$

for any function $f(r)$ and its Fourier transform $\tilde{f}(q)$, we obtain

$$\overline{\rho}_E(\mathbf{x},\mathbf{x}')=\left(\frac{2\pi me^2}{\varepsilon_0\hbar^2 k}\right)^2 K_0(xq_E)K_0(x'q_E)^* \times\int dz dz' e^{-iq_E(z-z')}S(\mathbf{r},\mathbf{r}',E). \tag{30}$$

Thus, given the *r* MDFF, we can calculate the density matrix of the inelastically scattered electron at the exit plane of the specimen. This may serve as a starting point for further processing, e.g., taking account of the contrast transfer function of the microscope in order to compute inelastic images, or the coherence between different points, an information particularly important in electron interferometry.

We can also estimate the ultimate resolution in energy filtered images. Even when the *r* MDFF is a delta function corresponding to a pointlike atom, the contrast would be limited by K_0. To calculate the contrast, we must define an upper limit for the momentum. Roughly, this can be identified with the cutoff wave number given by the Bethe ridge. This maximum limits the spatial resolution, and removes at the same time the infinity at $K_0(0)$. Figure 1 shows the contrast of a pointlike object for three values of q_E, corresponding to the Si plasmon energy, the Si-L ionization and the Si-K ionization, with the corresponding cutoff wave numbers. The plasmon and the L-edge signal shows very weak contrast according to the broad tail of the modified Bessel function K_0. Only the Si-K edge approaches the half width atomic dimensions. (The abscissa is in atomic units, i.e., Bohr radii.)

Note that example (a) should not be taken literally. The plasmon is collective in nature, contrary to our assumption of one-electron transitions. It is merely thought to elucidate the energy-loss dependence of the contrast.

In the next section, we discuss an example.

IV. ATOMIC CORE LOSSES: SI-K IONIZATION

The *r* MDFF for atomic core losses is important for simulation and interpretation of energy filtered element-specific images. We restrict the discussion to dipole-allowed transitions. They change the angular momentum quantum number by one unit.

A. The dipole approximation

For calculation of the density matrix ρ, we need Eqs. (8) and (21). For single atoms and core-level excitations an expansion of the wave functions into spherical harmonics yields[17]

$$S_{\mathrm{at}}(\mathbf{Q},\mathbf{Q}',E)=2(2l+1) \times\sum_{\lambda=0}^{\infty} P_\lambda(\cos\alpha)(2\lambda+1) \times\sum_{l'=0}^{\infty}(2\ell'+1)\begin{pmatrix}\ell & \lambda & \ell' \\ 0 & 0 & 0\end{pmatrix}^2 \times\langle j_\lambda(Q)\rangle_{n\epsilon'\ell\ell'}\langle j_\lambda(Q')\rangle_{n\epsilon'\ell\ell'}, \tag{31}$$

where

$$\langle j_\lambda(Q)\rangle_{n\epsilon'\ell\ell'}=\int dR u_{n\ell}(R)j_\lambda(QR)u_{\epsilon'\ell'}(R) \tag{32}$$

is a radial integral involving initial- and final-state radial wave functions and the spherical Bessel function. The variable α in the Legendre polynomial is the angle between $\mathbf{Q}$ and $\mathbf{Q}'$. The variable λ denotes the change of the angular momentum quantum number during the transition. At moderate scattering angles the term with $\lambda=1$ is most important.[18] These dipole-allowed transitions represent the largest contribution to the scattering cross section because the Lorentzian prefactor is large at small angles. It is therefore a good approximation for atomic transitions.

For the sake of simplicity, we now discuss such a dipole-allowed transition, say, from the 1*s* state of a silicon atom to a final state with *p*-wave symmetry right above the ionization edge at 1850 eV. According to the triangular property of the Wigner three-*j* symbols (: : :) Eq. (31) collapses to

$$S_{\mathrm{dip}}(\mathbf{Q},\mathbf{Q}',E)=6P_1(\cos\alpha)\langle j_1(Q)\rangle_{n\epsilon'01}\langle j_1(Q')\rangle_{n\epsilon'01}. \tag{33}$$

For the Si $1s\rightarrow\varepsilon'p$ transitions, the expectation value of the Bessel function can be approximated by

$$\langle j_1(Q)\rangle_{n\epsilon'01}\approx b(E)Qe^{-cQ^{1.5}}=b(E)f(Q). \tag{34}$$

The fit parameter for Si-K is $c\doteq 0.0234$, and b is an energy dependent normalization constant. Observing that $\cos\alpha=\mathbf{Q}\cdot\mathbf{Q}'/QQ'$, we can simplify Eq. (33) to

$$S_{\mathrm{dip}}(\mathbf{Q},\mathbf{Q}',E)\doteq a(E)\frac{\mathbf{Q}\cdot\mathbf{Q}'}{QQ'}f(Q)f(Q'). \tag{35}$$

The density matrix Eq. (21) of the fast electron after an energy loss via a dipole transition is then

$$\overline{\rho}_E(\mathbf{q}_x,\mathbf{q}_x')=a(E)\left(\frac{2\pi me^2}{\varepsilon_0\hbar^2 k}\right)^2\frac{\mathbf{Q}\cdot\mathbf{Q}'}{Q^3Q'^3}f(Q)f(Q'). \tag{36}$$

The dipole approximation[7] consists of replacing $f(Q)$ in Eqs. (35) and (36) by Q, i.e., the exponential factor is approximated by a step function

$$S(\mathbf{Q},\mathbf{Q}',E)=a(E)\Theta(Q-Q_c)\mathbf{Q}\cdot\mathbf{Q}'. \tag{37}$$

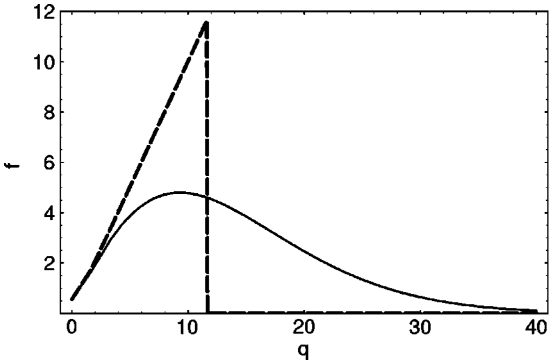

FIG. 2. The factor $f(Q)$ for dipole-allowed transitions (Si-K ionization), compared to the dipole approximation (dashed). Abscissa in atomic units, ordinate in arbitrary units.

This is a good approximation for small Q,Q'. How good is it for higher Q? Each of the two Q-dependent factors would then increase linearly up to the cutoff momentum Q_c; the maximum of the Bethe ridge $Q_c=\sqrt{2mE/\hbar^2}$ is a natural choice. (For Si-K, $Q_c=11.66$ atomic units). Figure 2 shows the exact q_x dependence of one factor and the dipole approximation. We see that it is only good for very small q_x. However, the cross section which is proportional to the diagonal element of the density matrix is quite well approximated (see Fig. 3, in logarithmic units). This is because the denominators in Eq. (36) intensify rapidly for higher Q.

B. Mutual coherence

An important consequence can be drawn from Eq. (36). We fix a direction $\mathbf{e}_q$ in the diffraction plane. This restricts the six-dimensional (6D) density matrix to a two-dimensional subspace (q,q'). The "1D density matrix" ρ_1 in this subspace still denotes the density or the mutual coherence, just along a fixed straight line through the center of the atom. For instance, the values on the skew diagonal of ρ_1 show the mutual coherence of the electron in directions $q,q'=-q$. Inspection of the skew diagonal, Fig. 4, tells us that electrons leaving in opposite directions relative to the direction of incidence are mutually coherent up to angles corresponding to much more than the cutoff momentum q_c. This coherence extending to high angles is responsible for the narrow charge distribution in r space, as we shall see.

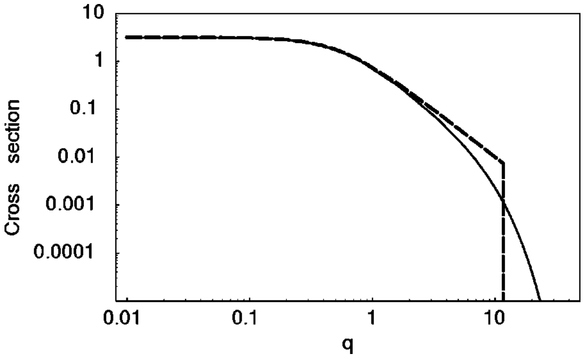

FIG. 3. Differential cross section $\propto f(Q)^2/Q^4$ for dipole-allowed transitions for Si-K ionization, compared to the dipole approximation (dashed). Abscissa in atomic units, ordinate in arbitrary units, both log scale.

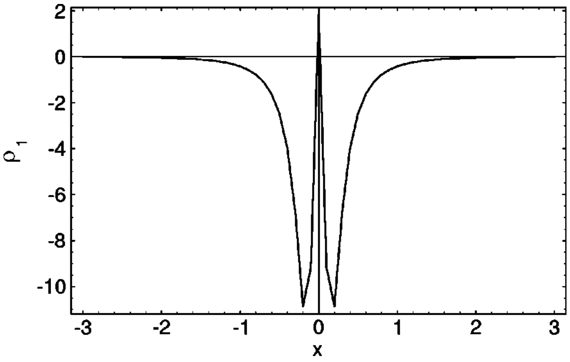

FIG. 4. Skew diagonal of the one-dimensional density matrix $\rho_1(q,q')$ for Si-K ionization, showing the mutual coherence in the diffraction plane. Abscissa in atomic units, ordinate in arbitrary units.

The scalar product $\mathbf{Q}\cdot\mathbf{Q}'$ causes the elements along the skew diagonal to become negative within a large range of momenta. This means that the phases of at least some electrons contained in the mixed state leaving at angles ϑ and $-\vartheta$ are shifted relative to each other. In dipole-allowed transitions, conservation of parity causes the probe electron to change parity since the scatterer does also. Consequently, the phase shift for dipole-allowed scattering on a single atom between scattering angles ϑ and $-\vartheta$ is π. This is a result that cannot be derived from inspection of the diffraction pattern which is radially symmetric.

C. The *r* MDFF

We derive now the r MDFF, by directly performing the Fourier transform of the MDFF for a dipole-allowed atomic transition of a Si 1s electron into the continuum. The MDFF, Eq. (35), factorizes into terms containing only $\mathbf{q}$ or $\mathbf{q}'$, so it suffices to evaluate

$$FT_{\mathbf{q}}\left[\frac{\mathbf{q}f(q)}{q}\right]=\int d^3q e^{i\mathbf{qr}}\frac{\mathbf{q}f(q)}{q}. \tag{38}$$

We chose $\mathbf{r}$ as z direction and give $\mathbf{q}$ in spherical coordinates. The Fourier transform is

$$FT_{\mathbf{q}}\left[\frac{\mathbf{q}f(q)}{q}\right]=\frac{1}{(2\pi)^3}\int q^2dq \times\int_0^{\pi}\sin\vartheta d\vartheta e^{iqr\cos\vartheta}\int_0^{2\pi}\frac{\mathbf{q}f(q)}{q}d\phi. \tag{39}$$

By performing the ϕ integral, the x and y components vanish for reasons of symmetry. There remains only the component parallel to $\mathbf{r}$. The vectorial property is retained: the Fourier transform of a vector field $\propto\mathbf{q}$ is a vector field $\propto\mathbf{r}$. With $\cos\vartheta=\xi$ the (ϑ,ϕ) integral is

$$2\pi\int_{-1}^{1}\xi e^{iqr\xi}d\xi=2\pi\frac{2i(\sin qr-qr\cos qr)}{(qr)^2}=2\pi g(qr) \tag{40}$$

and we obtain

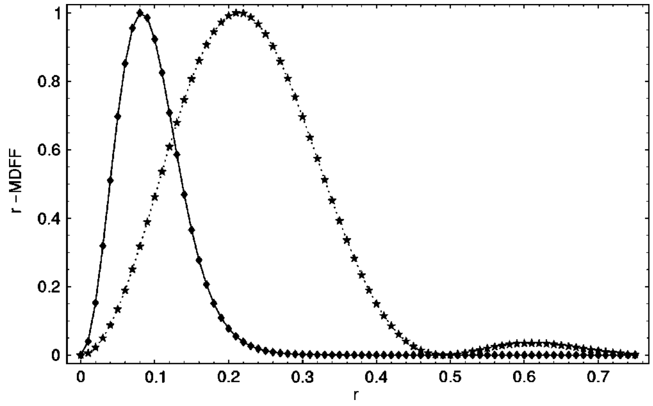

FIG. 5. r MDFF for Si-K ionization. Dipole-allowed transition (full line) and dipole approximation with cutoff momentum $q_c = 11.6$ a.u. Ordinate in arbitrary units.

$$FT_{\mathbf{q}}\left[\frac{\mathbf{q}f(q)}{q}\right]=\frac{\mathbf{r}}{r}\frac{1}{(2\pi)^2}\int q^2 g(qr)f(q)dq. \tag{41}$$

With the abbreviation

$$h(r)=\frac{1}{(2\pi)^2}\int_0^\infty q^2 g(qr)f(q)dq \tag{42}$$

the r MDFF reads

$$S(\mathbf{r},\mathbf{r}',E)=a(E)\frac{\mathbf{r}\cdot\mathbf{r}'}{rr'}h(r)h(r'). \tag{43}$$

We can compare this with Eq. (11) for an infinitely narrow range of initial energies, as is the case for core ionization,

$$S(\mathbf{r},\mathbf{r}',E)=\rho_{E_i}(\mathbf{r},\mathbf{r}')\rho_{E_i+E}(\mathbf{r}',\mathbf{r}). \tag{44}$$

For $\mathbf{r}=\mathbf{r}'$, this is the product of densities of the initial and the energetically allowed final states.

In dipole approximation, Eq. (37), the function $h(r)$ can be calculated in closed form, yielding

$$h(r)=\frac{1}{(2\pi)^2}\frac{[3-(q_c r)^2]\sin q_c r-3q_c r\cos q_c r}{(q_c r)^2}. \tag{45}$$

The r MDFF is a universal function of a dimensionless variable, scaling with the cutoff wave number q_c. Figure 5 compares exact results of the r MDFF with the dipole approximation, Eq. (45), for Si-K ionization. The cutoff wave number q_c was taken as the maximum of the Bethe ridge. (In atomic units, $q_c=\sqrt{2E}$.) The overestimation of the radial extension of the r MDFF is related to the fact that the dipole approximation underestimates the extension of $S(\mathbf{q},\mathbf{q}',E)$ by imposing a cutoff momentum. The so-induced discontinuity causes the oscillation seen at 0.6 a.u. The dipole approximation thus gives a radial extension of the r MDFF that is by a factor of two too large. As will be seen, this causes also an overestimation of the lateral dimension of the image of a single atom, by a slightly smaller factor of 1.5 (see Fig. 6). The oscillations seen in Figs. 5 and 6 are artifacts. However, when the outgoing electron is projected into an image plane by an objective lens, as is the case in electron microscopy, the collection aperture has a similar effect. In a 200 kV microscope, the cutoff momentum for the Si-K edge corresponds to a collection angle of ≈90 mrad. Spherical aberration would broaden the image and probably damp the oscillations.

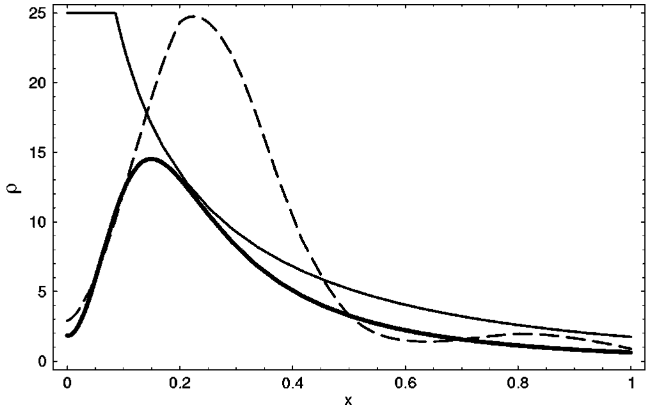

FIG. 6. Exit plane density of the outgoing fast electron for a Si-K dipole-allowed transition, compared to the modified Bessel function K_0 according to Eq. (28) (thin full line) and to the dipole approximation (dashed). Abscissa in atomic units, ordinate in arb. units.

D. The density matrix of the probe electron

In order to discuss the charge distribution in the exit plane of the specimen, we could use Eq. (27) and calculate the density matrix of the fast electron. Alternatively, one can transform directly from the two-dimensional diffraction plane. We do this for dipole-allowed transitions, as before.

Since the density matrix Eq. (36) factorizes into two terms depending on the primed respectively the nonprimed variables, its Fourier transform $\overline{\rho}(\mathbf{x},\mathbf{x}')$ does also. The Fourier transform of the first factor is

$$FT_{\mathbf{q}_x}\left[\frac{\mathbf{Q}f(Q)}{Q^3}\right]=iv\,\mathbf{e}_x+w\,\mathbf{e}_z. \tag{46}$$

Here, $\mathbf{e}_x$ is a unit vector in direction $\mathbf{x}$ in the exit plane, and $\mathbf{e}_z$ is perpendicular to the exit plane. The two functions are

$$v=\frac{1}{2\pi}\int_0^\infty \frac{q^2 J_1(qx)f(Q)}{Q^3}dq, \tag{47}$$

$$w=\frac{q_E}{2\pi}\int_0^\infty \frac{qJ_0(qx)f(Q)}{Q^3}dq, \tag{48}$$

[see Appendix C, Eqs. (C5)]. Since the Fourier transform of the second factor is the complex conjugate of that of the former, the inner product of the two vector fields is

$$\overline{\rho}_E(\mathbf{x},\mathbf{x}')=v(x)v(x')\mathbf{e}_x\cdot\mathbf{e}_{x'}+w(x)w(x'). \tag{49}$$

Note that the scalar product is $\mathbf{e}_x\cdot\mathbf{e}_{x'}=\cos\phi$ where ϕ is the angle between directions $\mathbf{x}$, $\mathbf{x}'$.

The terms in Eq. (49) factorize in x- and x'-dependent factors, but the sum does not. This shows, by the way, that a

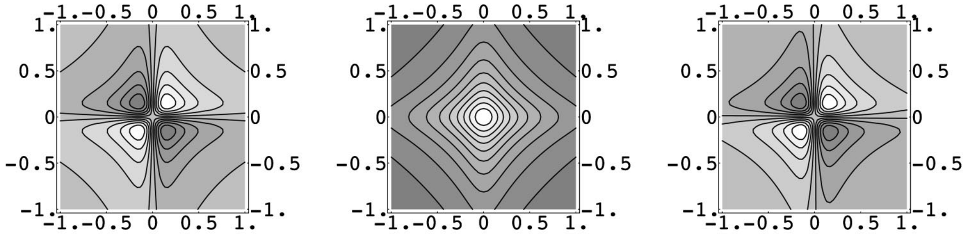

FIG. 7. Contour plot of the one-dimensional density matrix $\rho_1(x,x')$ of the outgoing electron in the exit plane of the specimen, after a Si-K ionization. Left: in-plane component v^2; middle: perpendicular component w^2; right: sum of both. Atomic units.

position measurement along a radial line as described by the 1D density matrix projects the fast electron onto a superposition of two pure states.

In the dipole approximation, the diagonal element of $\overline{\rho}_E(\mathbf{x},\mathbf{x}')$ is

$$\overline{\rho}_E(\mathbf{x},\mathbf{x}')=\frac{1}{(2\pi)^2}\left\{\left|\int_0^{q_c}\frac{q^2J_1(qx)}{Q^3}dq\right|^2+\left|\int_0^{q_c}\frac{q_e q J_0(qx)}{Q^3}dq\right|^2\right\}. \tag{50}$$

When we replace q_c by the momentum corresponding to the collection angle in the objective lens of an electron microscope, we obtain exactly the radial intensity in the image plane, as it was derived earlier for the image of a single atom by Kohl and Rose[7] and Berger and Kohl.[19] As these authors showed, decreasing the aperture would eventually remove the central dip, thus transforming the ring-shaped image into one with a central maximum.

Equation (49) renders the 1D density matrix

$$\rho_1(x,x')=v(x)v(x')+w(x)w(x'). \tag{51}$$

Its two components are shown for Si-K in Fig. 7. Note that the ''perpendicular'' term has a maximum at $x=0$ whereas the ''in plane'' term vanishes at $x=0$. This can be explained by the odd parity of the final p state. Another consequence is that the skew diagonal contains negative values—the wave function is anticorrelated with itself under inversion at the center. The perpendicular component is very small for Si-K. It does not much influence the overall shape of the density matrix as can be seen from a comparison of the in-plane (or parallel) component (left in the figure) with the sum (right in the figure). This is better visible in Fig. 8 which is a trace through the in-plane and perpendicular components along the main diagonal of $\rho_1(x,x')$, i.e., the density distribution of the outgoing wave field.

Figure 6 is a comparison between the densities obtained from the exact expression Eq. (36) and the dipole approximation Eq. (50) (dashed). The sharp cutoff induces oscillations which are missing in the exact expression. The maximum is shifted by $\approx 50\%$ to the right, i.e., the dipole approximation overestimates the spatial extension of the charge distribution after core-loss scattering. A similar effect was found in the r MDFF, Fig. 5. We also show a comparison of the rough estimate for pointlike scatterers, Eq. (28), already shown in Fig. 4(c), with the exact result. The charge-density distribution is narrower now than the exact result but is still a useful estimate for the ultimate spatial resolution that can be achieved in energy filtered atomic-resolution images. Outside the exact maximum, the distribution is well described, but contrast is overestimated by the modified Bessel function Eq. (28).

Figure 9 shows the directional autocorrelation function ac of the probe electron at the exit plane of the specimen

$$ac(x)=\int \rho_1(x+x',x')dx'. \tag{52}$$

For a pure state, this would indeed be $\int\psi(x+x')\psi^*(x')dx'$. Here x,x' are distances from the center of the atom, both taken along the same radial trace. It is important not to mix up the directional autocorrelation function with the usual one, also called internally folded density,[20] where the correlation integral is taken over three space.

From the figure, we see that the correlation length in the Si-K inelastic image is approximately 0.2 bohr radii.

V. CONCLUSIONS

We have shown that the MDFF is related to the density matrix of the excited target states in a simple manner. Equation (11) could be used to relate variations in the final-state wave functions caused by the crystal potential to details in the scattering cross section or in the off-diagonal terms of the MDFF. How these latter are accessible, at least partly, has been shown recently.[21,22]

We have explicitly given the solution of the kinetic equation for the density matrix of the probe electron in the single-scattering one-beam case. It makes possible the simulation of inelastic scattering cross sections and energy filtered high-

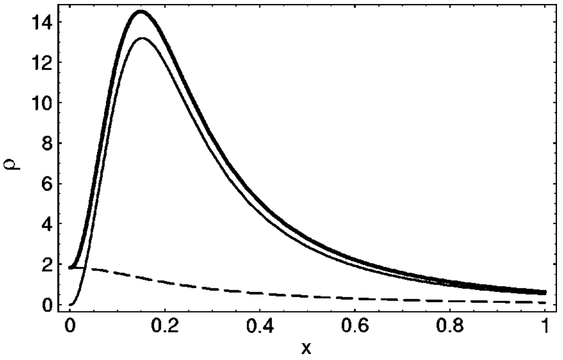

FIG. 8. Exit plane density of the outgoing fast electron (thick full line), its in-plane component v^2 (thin full line), and its perpendicular component w^2 (dashed). Units are as in Fig. 6. .

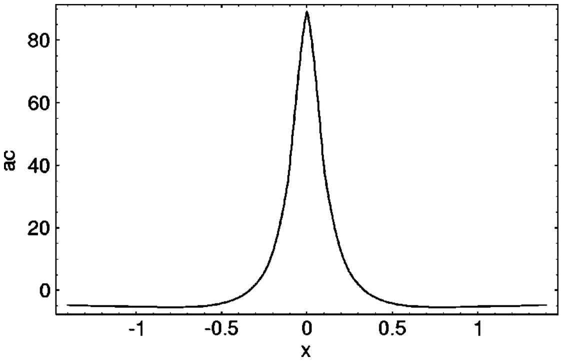

FIG. 9. Autocorrelation function $ac(x)$, Eq. (52) for Si-K ionization. Units as in Fig. 8.

resolution electron micrographs within the same framework and the same approximations. The advantage is that both image and diffraction information is available at the same time to be compared with experiments. As shown recently,[16] the dynamical effects after the inelastic interaction introduce phase contrast anew, a fact that makes interpretation of filtered high-resolution images more difficult when the specimen is thicker than roughly a third of the extinction distance of the Bragg reflections that contribute to the image. However, for very thin specimens the proposed solution should still hold.

The contrast in inelastic images can be estimated via the modified Bessel functions in order to judge whether a particular ionization edge is suitable for imaging. The concept of the 1D density matrix allows to interpret the coherence properties of the inelastically scattered probe electron in the most direct way. In imaging, we would have almost incoherent conditions. This fact should facilitate interpretation of energy filtered images since phase contrast plays a minor role.

Besides taking account of dynamical diffraction conditions (as mentioned above), two generalizations appear straightforward: (1) inclusion of the effect of the objective lens, and (2) extension to L-shell ionization and to dipole-forbidden transitions.

ACKNOWLEDGMENTS

P.S. thanks S. L. Dudarev for his kinetic equation and for valuable suggestions concerning its solution. Thanks are due to the École Centrale Paris, especially to Ph. Bompard for the financing of a stay in Paris where part of this work was done. M.N. acknowledges support of the European Union under TMR Contract No. ERBFM-BICT961416. Part of this work was financially supported by the Austrian Fonds zur Förderung der wissenschaftlichen Forschung, under Project No. P10408-PHY.

APPENDIX A

We first transform the kinetic Eq. (17) in the plane $\mathbf{R}$ perpendicular to $\mathbf{k}_0$:

$$\begin{aligned} N\rho_E(\mathbf{q}_x,\mathbf{q}_x',r_z,r_z') &= \int d^2R\,d^2R'\,e^{-i(\mathbf{q}_x\mathbf{R}-\mathbf{q}_x'\mathbf{R}')}\rho_E(\mathbf{r},\mathbf{r}') \\ &= \int d^3x\,d^3x'\,FT_{\mathbf{R}}[G_k(\mathbf{r},\mathbf{x})]FT_{-\mathbf{R}'} \\ &\quad\times[G_k(\mathbf{r}',\mathbf{x}')^*]K(\mathbf{x},\mathbf{x}',E)\rho_0(\mathbf{x},\mathbf{x}'). \end{aligned} \tag{A1}$$

The two-dimensional Fourier transform of the free particle's Green function,

$$G_k(\mathbf{r},\mathbf{x}) = -\frac{m}{2\pi\hbar^2}\frac{1}{|\mathbf{r}-\mathbf{x}|}e^{ik|\mathbf{r}-\mathbf{x}|}, \tag{A2}$$

where $k^2=2mE/\hbar^2$, is[8]

$$FT_{\mathbf{R}}[G_k(\mathbf{r},\mathbf{x})] = \frac{-im}{\hbar^2|k_z|}e^{-i\mathbf{q}_x\mathbf{x}}e^{ik_z(r_z-x_z)}, \tag{A3}$$

where $k_z=\sqrt{k^2-q_x^2}$. Observing that $FT_{-r}[G^*]=FT_r[G]^*$, and inserting the density matrix of the incident electron ρ_0, Eq. (19), we find

$$\begin{aligned} \rho_E(\mathbf{q}_x,\mathbf{q}_x',r_z,r_z') = {} & \frac{m^2}{\hbar^4k_z^2}e^{ik_z(r_z-r_z')} \\ & \times\int d^3x\,d^3x'\,e^{-ik_z(x_z-x_z')}e^{-i(\mathbf{q}_x-\mathbf{k}_0)\mathbf{x}} \\ & \times e^{i(\mathbf{q}_x'-\mathbf{k}_0)\mathbf{x}'}K(\mathbf{x},\mathbf{x}',E). \end{aligned} \tag{A4}$$

The integral is recognized as the double Fourier transform of the inelastic scattering function K, Eq. (18), at positions

$$\mathbf{Q}=\begin{pmatrix}\mathbf{q}_x\\ k_z-k_0\end{pmatrix}\mathbf{Q}'=\begin{pmatrix}\mathbf{q}_x'\\ k_z-k_0\end{pmatrix}, \tag{A5}$$

i.e.,

$$\rho_E(\mathbf{q}_x,\mathbf{q}_x',r_z,r_z') = \frac{m^2e^4}{\hbar^4k_z^2\varepsilon_0^2}\frac{S(\mathbf{Q},\mathbf{Q}',E)}{Q^2Q'^2}e^{ik_z(r_z-r_z')}. \tag{A6}$$

For small scattering angles, $k_z\approx k$. $k-k_0$ is the negative difference of radii of the Ewald spheres before and after inelastic scattering. For small energy losses $E\ll E_0$ we may approximate $k-k_0\approx -k_0E/2E_0 := q_E$.

Now the transform with respect to r_z,r_z' is performed:

$$\rho_E(\mathbf{q},\mathbf{q}') = \frac{m^2e^4}{\hbar^4k_z^2\varepsilon_0^2}\frac{S(\mathbf{Q},\mathbf{Q}',E)}{Q^2Q'^2}FT_{r_z,-r_z'}[e^{ik_z(r_z-r_z')}]. \tag{A7}$$

The Fourier transforms of the exponentials are $4\pi^2\delta(q_z-k_z)\delta(q_z'-k_z)$. Integration of Eq. (A7) over the unobserved variables q_z,q_z' yields eventually

$$\overline{\rho_E}(\mathbf{q}_x,\mathbf{q}_x') = \left(\frac{2\pi me^2}{\varepsilon_0\hbar^2k_z}\right)^2\frac{S(\mathbf{Q},\mathbf{Q}',E)}{Q^2Q'^2}. \tag{A8}$$

APPENDIX B

We calculate

$$FT_{\mathbf{q}_x}[(q_x^2+q_E^2)^{-1}]=\frac{1}{(2\pi)^2}\int e^{i\mathbf{x}\mathbf{q}_x}\frac{1}{(q_x^2+q_E^2)}d^2q_x. \tag{B1}$$

In cylindrical coordinates φ, ρ, where φ is the angle between $\mathbf{x}$ and $\mathbf{q}_x$, this is

$$\begin{aligned}FT_{\mathbf{q}_x}[(q_x^2+q_E^2)^{-1}]&=\frac{1}{(2\pi)^2}\int_0^\infty d\rho\,\frac{\rho}{(\rho^2+q_E^2)}\int_{-\pi}^{\pi}d\varphi e^{ix\rho\cos\varphi}\\&=\frac{1}{2\pi}\int_0^\infty d\rho\,\frac{\rho}{(\rho^2+q_E^2)}J_0(\rho x)=K_0(q_Ex).\end{aligned} \tag{B2}$$

J_0, K_0 are the Bessel function and the modified Bessel function of order zero.

APPENDIX C

For integration, we choose the x axis of the $\mathbf{q}$ space parallel to $\mathbf{x}$. In cylindrical coordinates the unit vector $\mathbf{Q}/Q$ reads

$$\frac{\mathbf{Q}}{Q}=\frac{1}{Q}\begin{bmatrix}q\cos\phi\\q\sin\phi\\q_e\end{bmatrix}. \tag{C1}$$

The Fourier transform Eq. (46) is

$$\begin{aligned}&\frac{1}{(2\pi)^2}\int d^2q_xe^{i\mathbf{q}_x\mathbf{x}}\begin{bmatrix}q\cos(\phi)\\q\sin(\phi)\\q_e\end{bmatrix}\frac{f(Q)}{Q^3}\\&=\frac{1}{(2\pi)^2}\int qdq\int_0^{2\pi}d\phi\,e^{iqx\cos\phi}\begin{bmatrix}q\cos(\phi)\\q\sin(\phi)\\q_e\end{bmatrix}\frac{f(Q)}{Q^3}.\end{aligned} \tag{C2}$$

The ϕ integral is done separately for the three components: For the first component (in x direction) we substitute $\cos\phi=\xi$. This yields

$$\frac{i}{2\pi}J_1(qx). \tag{C3}$$

The second component vanishes for reasons of symmetry. The z component is

$$\frac{1}{2\pi}J_0(qx). \tag{C4}$$

The q integral is therefore a vector with components parallel to $\mathbf{x}$ and to z:

$$FT_{\mathbf{q}_x}\left[\frac{\mathbf{Q}f(Q)}{Q^3}\right]=iv\mathbf{e}_x+w\mathbf{e}_z,$$

$$v=\frac{1}{2\pi}\int_0^\infty\frac{q^2J_1(qx)f(Q)}{Q^3}dq,$$

$$w=\frac{q_E}{2\pi}\int_0^\infty\frac{qJ_0(qx)f(Q)}{Q^3}dq. \tag{C5}$$

The Fourier transform of the second factor of the density matrix is with respect to $-q'$. This is the complex conjugate of the former integral, that is, v changes sign, and w is identical to the previous result.

---

[1] Y. Kainuma, Acta Crystallogr. **8**, 247 (1955).

[2] J. Gjønnes, Acta Crystallogr. **20**, 240 (1966).

[3] P. Rez, C. J. Humphreys, and M. J. Whelan, Philos. Mag. **35**, 81 (1977).

[4] F. N. Chukhovskii, L. A. Alexanjan, and Z. G. Pinsker, Acta Crystallogr., Sect. A: Cryst. Phys., Diffr., Theor. Gen. Crystallogr. **29**, 38 (1973).

[5] D. K. Saldin, Philos. Mag. B **56**, 515 (1987).

[6] L. J. Allen, Ultramicroscopy **48**, 97 (1993).

[7] H. Kohl and H. Rose, Adv. Electron. Electron Phys. **65**, 173 (1985).

[8] S. L. Dudarev, L. M. Peng, and M. J. Whelan, Phys. Rev. B **48**, 13 408 (1993).

[9] L. D. Landau, Z. Phys. **45**, 430 (1927).

[10] J. von Neumann, Göttinger Nachr. **1**, 246 (1927).

[11] D. ter Haar, Rep. Prog. Phys. **24**, 304 (1961).

[12] K. Blum, *Density Matrix: Theory and Application* (Plenum, New York, 1981).

[13] P. Schattschneider, *Fundamentals of Inelastic Electron Scattering* (Springer, Wien, 1986).

[14] D. D. Vvedenski, in *Unoccupied Electronic States*, edited by J. C. Fuggle and J. E. Inglesfield (Springer, Berlin, 1992), p. 139.

[15] C. Rossouw, S. L. Dudarev, T. W. Josefsson, and L. J. Allen, Ultramicroscopy **72**, 17 (1998).

[16] P. Stallknecht and H. Kohl, Ultramicroscopy **66**, 261 (1996).

[17] M. Nelhiebel, N. Luchier, P. Schorsch, P. Schattschneider, and B.

Jouffrey, Philos. Mag. B (to be published).

[18] S. T. Manson, Phys. Rev. A **6**, 1013 (1972).

[19] A. Berger and H. Kohl, Microsc. Microanal. Microstruct. **3**, 159 (1992).

[20] A. J. Thakkar, A. C. Tanner, and V. H. Smith, in *Density Matrices and Density Functionals*, edited by R. Erdahl and V. H. Smith (Reidel, Dordrecht, 1987), pp. 327–337.

[21] P. Schattschneider, B. Jouffrey, and M. Nelhiebel, Phys. Rev. B **54**, 3861 (1996).

[22] M. Hölzl, P. Schattschneider, M. Nelhiebel, B. Jouffrey, and F. Hofer, Inst. Phys. Conf. Ser. **153**, 171 (1997).